THE ASTROPHYSICAL JOURNAL, 378:763–772, 1991 September 10

MEASUREMENT OF COSMIC-RAY PROTON AND HELIUM SPECTRA DURING THE 1987 SOLAR MINIMUM

E. S. SEO,[1,2] J. F. ORMES,[1] R. E. STREITMATTER,[1] S. J. STOCHAJ,[1] W. V. JONES,[2] S. A. STEPHENS,[3] AND T. BOWEN[4]

Received 1991 January 23; accepted 1991 March 26

ABSTRACT

The differential cosmic-ray proton and helium spectra have been measured during the 1987 solar minimum using a balloon-borne superconducting magnetic spectrometer launched from Prince Albert, Canada. The changing geomagnetic cutoff along the balloon trajectory was observed in the low-energy proton data to be about 25% below the nominal calculated values. The absolute particle fluxes were approximately equal to the highest fluxes observed at the previous solar minimum in 1977. Above 10 GV the observed spectra are represented by a power law in rigidity with spectral indices of 2.74 ± 0.02 for protons and 2.68 ± 0.03 for helium. The measurements above 200 MeV per nucleon are consistent with rigidity power-law interstellar spectra modulated with the solar modulation parameter $\phi = 500$ MV. The energy dependence of the proton-to-helium ratio is consistent with rigidity power-law injection spectra and rigidity-dependent propagation without reacceleration.

Subject headings: cosmic rays: general — particle acceleration

1. INTRODUCTION

Proton and helium nuclei are the two dominant cosmic-ray components, so the study of their spectral shapes and relative abundance is the basis for understanding particle propagation in interstellar space and particle acceleration in the source region. The absolute fluxes at solar minimum provide the closest approximation to those in the local interstellar medium outside the heliosphere. Fluxes in the interstellar medium, determined by demodulating the locally measured spectra, contain information about the role that cosmic rays play in Galactic dynamics. The relative spectra of protons and helium nuclei, with different rigidities at constant velocity, can place significant constraints on the modulation process.

Theories of cosmic-ray acceleration in the Galaxy have focused on first-order Fermi acceleration in strong shocks occurring in the shells of supernova or in the surrounding interstellar medium (Bell 1978a, b; Blandford & Ostriker 1978). The resulting injection spectra in momentum space have a power law of the form $F(p) \propto p^{-\gamma}$, where $\gamma = -(2 + \epsilon)$, p is momentum, and ϵ (determined by the characteristics of the shock) is between 0.1 and 0.3. This spectral form is expected to apply to a wide range of energies from approximately a few GeV to a few TeV. At lower energies, the spectra will be modified by details of the injection process, escape from the source, and ionization loss processes. At higher energies, the scale size of the acceleration region will eventually modify the spectra (Webber, Golden, & Stephens 1987). Specific models have been used to examine the acceleration process together with subsequent Galactic propagation and to predict the spectra of particles arriving at the solar system (Blandford & Ostriker 1980; Kota & Owens 1980; Ip & Axford 1985).

The realization that the interstellar medium is a very turbulent environment driven to a large degree by the action of stellar winds, supernovae, and their shock waves has led to the idea of reacceleration during cosmic-ray propagation. Reacceleration in interstellar space has been studied in recent years to examine its effect on the secondary components of cosmic rays (Silberberg et al. 1983). The observed spectral shape of secondary nuclei, which is steeper than that of primary nuclei, suggests that Galactic cosmic rays probably gain most of their energy during a single acceleration and do not encounter repeated increments of strong acceleration during their lifetime (Blandford & Ostriker 1980; Cowsik 1980; Fransson & Epstein 1980; Eichler 1980). Nevertheless, it seems likely that cosmic rays could encounter a number of weak shocks during their propagation through the interstellar medium, and one needs to examine such effects on all cosmic-ray components (Stephens & Golden 1990).

The Low Energy Antiproton (LEAP) balloon flight experiment (Streitmatter et al. 1989) provided an opportunity to measure the proton and helium spectra over the wide energy range from 200 MeV per nucleon to 100 GeV per nucleon with a single instrument. The balloon was launched from Prince Albert, Saskatchewan, Canada on 1987 August 21, soon after the 1987 March cosmic-ray intensity maximum between the 21st and 22nd solar cycle (Shea & Smart 1990). It spent more than 20 hr at its float altitude of about 36 km with residual atmospheric overburden of 4.7 g cm^{-2}, and its trajectory moved over the nominal geomagnetic cutoff range 0.66–1.10 GV.

The data collected during the latter part of the flight contained a significantly larger fraction of atmospheric secondaries than the data from the early part of the flight. This information was used in the analysis of the low-energy antiproton spectrum, which was the primary objective of the LEAP experiment (Streitmatter et al. 1990). In this paper we present the results from analysis of the proton and helium spectra, specifically their absolute fluxes, the effects of the geomagnetic cutoff and solar modulation on the low-energy

[1] NASA/Goddard Space Flight Center, Code 661, Greenbelt, MD 20771.
[2] Department of Physics and Astronomy, Louisiana State University, Baton Rouge, LA 70803-4001.
[3] Particle Astrophysics Laboratory, New Mexico State University, Las Cruces, NM 88003.
[4] Department of Physics, University of Arizona, Tucson, AZ 85721.

proton spectra below about 10 GeV per nucleon, and the spectral indices for protons and helium over the rigidity range 10–100 GV.

2. EXPERIMENTAL PROCEDURE

2.1. *The LEAP Instrument*

The LEAP instrument, illustrated in Figure 1, consisted of three principal components: a superconducting magnet spectrometer with a multiwire proportional counter (MWPC) tracking system; a time-of-flight (TOF) system; and a liquid Cherenkov detector. The magnet was based on a single coil of copper-clad NbTi wire, with 61 cm outer diameter, 36 cm inside diameter, and 10 cm axial thickness. It produced a magnetic field of 33 kG at the center of the coil when operating at a current of 100 A. This somewhat reduced current was chosen to increase stability in the LEAP flight.

The MWPC stack consisted of eight identical 50 × 50 cm^2 chambers with a total separation of 110 cm. The positions of incoming particles were obtained from the arrival time of the signals at each end of the delay lines. All eight planes provided position measurements in the x-direction (perpendicular to the magnet axis), and four measurements were made in the y-direction (parallel to the magnet axis). Multiparticle detection and general consistency checking were carried out by demanding that the sum of the two arrival times equaled the time required for a signal to travel the length of the delay line (Golden et al. 1978).

The TOF system consisted of 20 Bicron 404, 1 cm thick plastic scintillator paddles, each of which was viewed end-on by a Hamamatsu R2490-1 photomultiplier tube (PMT), which was selected because its fine-mesh electron transmissive dynode permits it to function unshielded in high magnetic fields (Takasaki, Ogawa, & Tobimatsu 1985). The paddles were grouped into four timing planes, T1–T4. The T1 and T2 planes "stacked" at the top of the detector constituted the entrance detector of the telescope, while T3 and T4 constituted the exit detector. Each of the top planes (T1, T2) consisted of six paddles, each of which was, in turn, viewed by one PMT. The lower planes (T3, T4) each consisted of four paddles, separated by about 1.8 m from the top planes; this distance corresponds to ~6 ns at the speed of light. The paddle lengths ranged from 60 to 110 cm, and the paddle widths ranged from 14 to 20 cm.

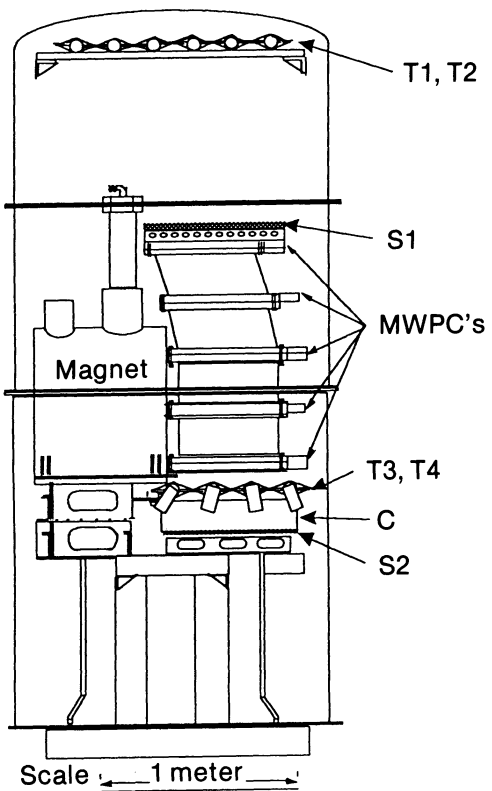

FIG. 1.—Schematic diagram of the LEAP apparatus

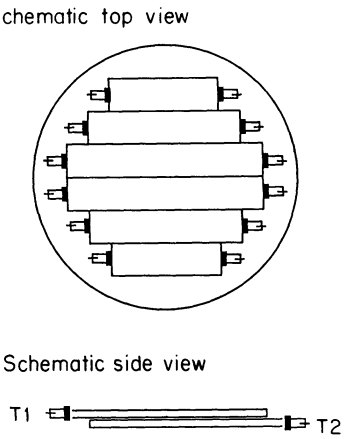

FIG. 2.—Top and side view of the timing scintillator paddles

Figure 2 shows the top and side view of the timing paddles. Dual, independent measurements in each TOF plane (T1–T4) minimized the dispersion in both the energy loss and the TOF measurements. The signal from only one end of each paddle was read out, so a charged particle passing through the entrance plane had to pass through two independent scintillators, i.e., the "stacked" paddle pair T1 and T2. The flight time between planes was determined with 250 ps resolution. The timing improvement achieved by this novel technique depends on the extent to which conventional double-ended measurements are influenced by correlated uncertainties, e.g., light path–dependent effects and extreme Landau fluctuations (Stochai 1990).

The timing data from the TOF system permitted separation of downward-moving protons from splash albedo. During data analysis, the requirement that only one pair of stacked paddles be hit at the entrance plane removed unwanted background, and the particle position in the TOF planes determined from timing was required to agree with the position derived from the tracking detector. In addition to the TOF system, two other scintillators, S1 and S2, were used to determine the incident charge and to make a redundant TOF measurement sufficient for separating upward and downward moving particles.

The Cherenkov counter consisted of a 43.8 × 43.8 × 12.7 cm^3 clear plastic acrylic box filled with the liquid fluorocarbon FC-72. The refractive index of 1.25 for the liquid FC-72 resulted in a threshold velocity $\beta_{th} = 0.8$. The FC-72 radiator, which was viewed by 16 Hamamatsu R2490 PMTs, provided redundant velocity measurements for 0.6–1.6 GeV per nucleon particles (Moats 1989).

Triggering of the LEAP instrument occurred whenever a particle traversed at least one paddle in each of the four

scintillator-paddle layers (T1–T4), thereby producing the coincidence trigger and initiating the event readout by the onboard data processing electronics. The onboard computer required a nonzero signal in the S1 scintillator to eliminate some unwanted events and to limit the data rate. The timing-start signal was derived from the bottom scintillator paddle set, T4, located below the spectrometer.

The payload was inhibited from recognizing any additional events from the time of the coincidence trigger until the digitization was complete. The dead time, which is the time lost while the payload modules and computer are busy reading out an event, was measured by a clock that was enabled when the coincidence was registered and disabled when readout was complete. The total accumulated time in the clock was regularly transmitted to the ground as part of the engineering data frame.

2.2. *Data Analysis*

Approximately 10^7 triggers were recorded during the flight. The analysis procedure was designed to select legitimate protons and helium nuclei and to measure their rigidity with the best possible accuracy. Helium nuclei were selected with the same criteria as protons, except for their different ionization rates.

The pulse-height information from T1, T2, S1, T3, and T4 was corrected for position dependence by selecting relativistic particles and measuring their mean pulse height as a function of position. The correction factors were derived iteratively, and both proton and helium nuclei were used for the position mappings. The charge separation is shown in the plot of corrected Z^2 versus log R in Figure 3. Events having positive rigidity and ionization corresponding to singly charged particles in T1 and T2 included protons, kaons, pions, muons, and positrons. The TOF system and rigidity information from the MWPCs permitted separation of protons from the low-mass particles in the low-rigidity region up to ~ 1 GV. At higher rigidities, the proton data sample included negligible contributions from the low-mass particles.

The determination of particle rigidity began with transformation of the raw MWPC data into measured track coordinates in a three-dimensional coordinate system. The relative locations of the chambers were determined from a multiparameter minimizing routine that provided the best fits to straight line trajectories (Golden et al. 1973). The straight tracks were obtained by operating the instrument with the magnet off. Once the spectrometer was aligned, particle rigidities could be determined from a least-squares fit to the measured points (Adams 1972; Golden et al. 1990). For each trajectory, a computer program integrated the equation of motion using a precalculated magnetic field map. The fit was tested by computing the deviations between the measured points and the computed trajectory. Proton and helium events meeting the following criteria were slected for spectral analysis: (1) the MWPC tracking data was sufficient to reconstruct the trajectory; (2) at least six chambers for the x-direction and three chambers for the y-direction had usable information with good resolution; and (3) the goodness of fit χ^2 per degree of freedom was less than 10 for both x and y.

The track registration efficiency for a given MWPC was defined as the relative number of hits in that chamber to the total number of good events. In practice, however, the efficiency ϵ_i of chamber i was determined from the ratio r_i of the number of events that missed that chamber to the number of events that hit all the chamber planes, i.e., $\epsilon_i = 1/(1 + r_i)$. Several subsets of the data were analyzed to check whether the chamber efficiencies exhibited any charge or energy dependence, but no such dependencies were found. The average chamber efficiency was about 95%.

Magnetic deflection, the inverse of the particle rigidity, is proportional to the spatial curvature, so its error distribution is related to the position measurement error distribution. To minimize the contribution of multiple Coulomb scattering to this error distribution, low-energy particles were removed using the TOF and FC-72 Cherenkov counter data. Figure 4 shows the deflection distribution obtained by operating the

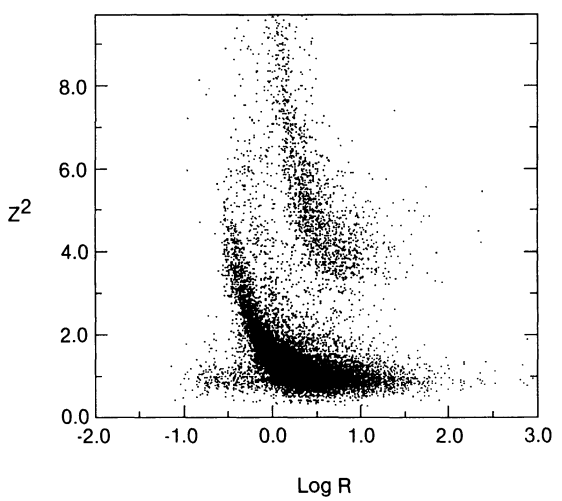

FIG. 3.—Charge distribution, z^2 ($\beta = 1$) vs. log R, for a sample of the data

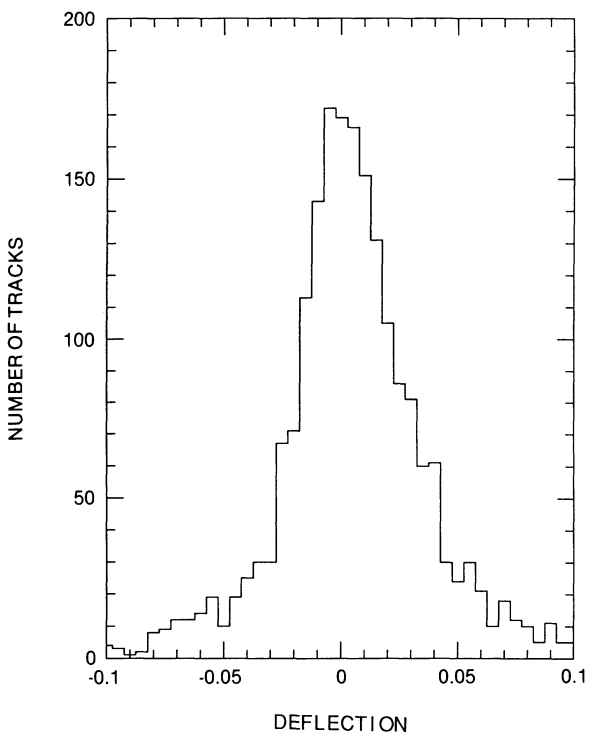

FIG. 4.—Deflection distribution for events with the magnet off at the end of the flight.

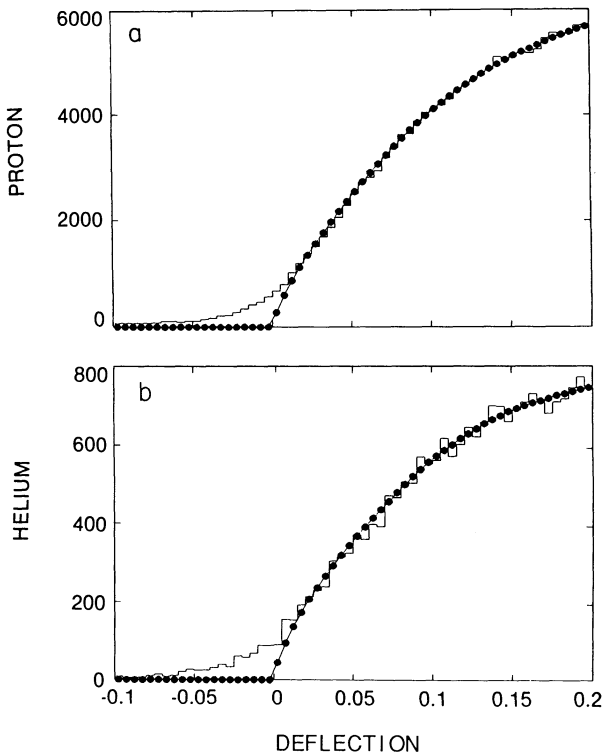

FIG. 5.—Deflection distribution of (*a*) protons and (*b*) helium before (*stepped histogram*) and after (*filled circles*) deconvolution.

instrument with the magnet off at the end of the flight. This distribution was taken to be the resolution function for the instrument, and its center was taken to be the zero deflection point. The standard deviation (σ) of the Gaussian fit to the central part of this error distribution is 0.018, which indicates an approximate maximum detectable rigidity ($1/\sigma$) of ~ 56 GV for the raw rigidity measurement.

The finite spectrometer resolution caused spillover among the rigidity bins, which in turn distorted the measured spectra, especially in the high-energy region. Since the measured spectra are convolutions of the input spectra and the inherent resolution function, the true input spectra could be obtaind by deconvolution, assuming the absence of any additional noise. The resolution matrix was comprised of a set of row vectors representing the resolution function centered at each deflection bin. The deconvolution process required multiplying the inverse of the resolution matrix by the column vector representing the measured spectra (Seo 1991). The deflection distributions of protons and helium before and after the deconvolution process are shown in Figure 5. The spillover to the negative deflection region has been removed by deconvolution, which in effect extended the reliable rigidity range to at least 100 GV.

3. RESULTS

3.1. *Geomagnetic Cutoff Effects*

The theory of charged particle motion in the geomagnetic field predicts that cosmic rays with a magnetic rigidity below a certain value, R_c, will be deflected enough to miss Earth entirely for a given direction. This smallest momentum at

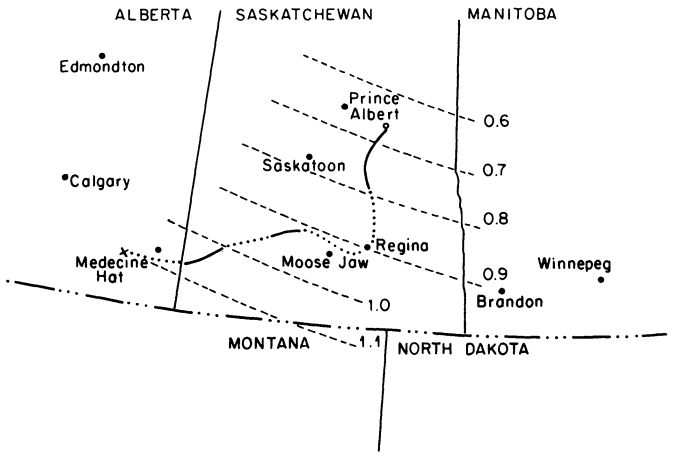

FIG. 6.—Trajectory of the balloon flight

which all directions are allowed, i.e., the geomagnetic cutoff, increases rapidly as latitude decreases.

The effects of the varying geomagnetic cutoff were observed in the proton data collected along the balloon trajectory, which is illustrated in Figure 6; also shown are the dashed lines of constant nominal cutoff rigidity in GV (Shea & Smart 1983). The solid lines along the trajectory identify three intervals (so-called start, middle, and end of the flight) used for the low-energy spectral analysis discussed below. The LEAP instrument was launched near 254°.0 W longitude and 53°.0 N latitude, where, according to the tables of Shea & Smart (1983), the nominal geomagnetic cutoff rigidity is $R_c = 0.65$ GV. After more than 20 hr floating generally southward and westward, the flight was terminated in the vicinity of Medicine Hat, Alberta, Canada near 249°.4 W longitude and 50°.5 N latitude, where $R_c = 1.11$ GV.

The proton spectra from the start and end of the flight are compared in Figure 7*a*. The Barkas & Berger (1964) range-energy tables were used to extrapolate the differential energy spectra to the top of the atmosphere. The instrumental range cutoff can be seen at ~ 0.45 GV. The observed spectrum results from the superposition of two spectra: the primary proton spectrum with the geomagnetic cutoff and the atmospheric secondary spectrum, which decreases with increasing rigidity. The difference between the spectra observed near the start and the end of the flight reflects the varying geomagnetic cutoff.

As shown in Figure 7*b*, the primary proton spectrum was obtained by subtracting the secondary proton spectrum at 5 g cm^{-2} calculated by Rygg & Earl (1971) from the measured spectrum at the top of the LEAP instrument. The normalization for the secondary proton spectrum was obtained by matching the initial and final spectra at high (>few GV) rigidities.

Figure 7*c* shows the primary proton spectra at the top of the atmosphere for the three intervals along the balloon trajectory identified by the solid lines in Figure 6, i.e, near the start, middle, and end of the flight. The "measured" geomagnetic cutoffs in these intervals were taken to be the values where the primary protons were 50% of their values in the absence of any cutoffs. As shown by the comparison in Table 1, these values are approximately 25% below the nominal cutoffs expected from detailed orbit calculations based on Earth's surface field (Shea & Smart 1983), but they generally agree with earlier observations (Bingham et al. 1968; McDonald 1957).

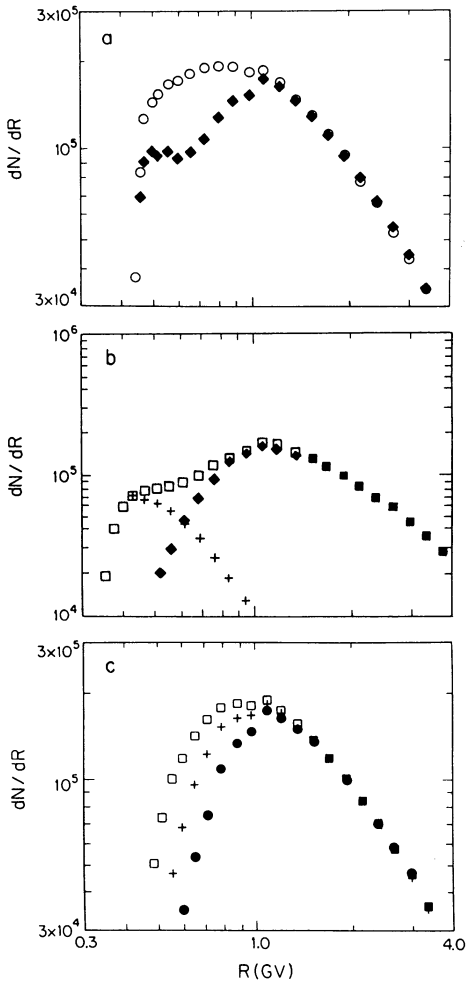

FIG. 7.—(*a*) Proton spectra at the top of the atmosphere for the "start" (*open circles*) and "end" (*filled diamonds*) of the flight. (*b*) Three proton spectral components: observed spectrum at the end of the flight (*open squares*); calculated spectrum of atmospheric secondaries (*plus signs*); primary spectrum = observed spectrum − spectrum of secondaries (*filled diamonds*). (*c*) Primary protons at the top of the atmosphere for the "start" (*open squares*), "middle" (*plus signs*), and "end" (*filled circles*) of the flight.

The nominal geomagnetic cutoff is an effective cutoff based on an average of the Stormer and main-cone vertical cutoffs. The penumbral width at the location of our measurement was 8%–12% of the nominal cutoff. The nonvertical direction cutoff seen by the ~23° opening angle of the LEAP spectrometer could be 2%–3% lower or higher than the vertical cutoff, depending on whether the incident particle arrived from the east or west. Consequently, the observed cutoff for an isotropic flux centered on the vertical would generally be less than the vertical cutoff. Furthermore, the observed cutoffs are not sharp (Pennypacker et al. 1973), probably reflecting some inrinsic geomagnetic effects (Webber & McDonald 1964). Smart, Shea, & Gall (1969) tried to explain the discrepancy between the observation of Bingham et al. (1968) and their calculated cutoffs by taking into account extraterrestrial currents. It should be noted that no geomagnetic storm activity was reported for the period of the LEAP flight.

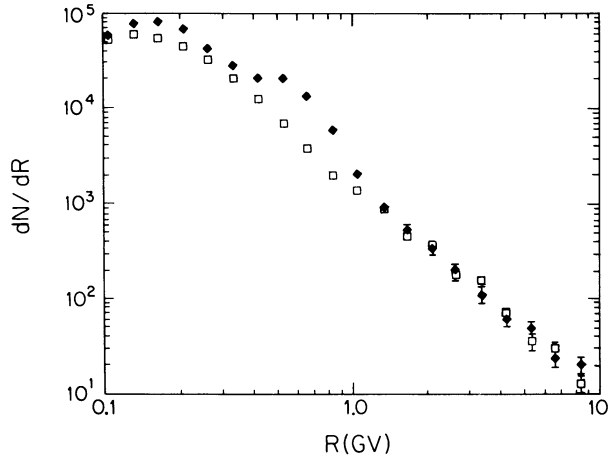

FIG. 8.—Splash albedo spectra for $z = +1$ (*filled diamonds*) and $z = -1$ particles (*open squares*).

3.2. *Splash Albedo*

The timing data from the TOF counters permitted determination of the splash albedo, which often constitutes an unwanted background for balloon experiments. Splash albedo protons were selected with the same criteria as protons, except for their negative track deflection and negative velocity (upward-moving) direction. Figure 8 shows the observed splash albedo spectra for singly charged particles, including protons, kaons, pions, muons, and electrons. Using the TOF to identify protons, it was found that the bump just below 1 GV in the $z = +1$ albedo spectrum is due to the proton component. Table 2 summarizes the observed ratios of albedo protons to downward moving protons as a function of rigidity. This ratio decreases with rigidity as approximately R^{-4}.

3.3. *Differential Energy Spectra*

The total number of measured nuclei of a given species is proportional to the instrument geometric factor (330 cm^2 sr for LEAP) and the measurement time, T, which must be corrected for the dead time; the ratio of dead time to real elapsed time was about 0.3 for LEAP. In addition, the overall instrument efficiency must be known to obtain the absolute fluxes.

TABLE 1

COMPARISON OF THE NOMINAL AND MEASURED CUTOFFS ALONG THE LEAP TRAJECTORY

Parameter	Start	Middle	End
Interval start	255.7 E, 52.7 N	253.3 E, 50.7 N	251.0 E, 50.3 N
Interval stop	255.5 E, 51.5 N	252.5 E, 50.7 N	250.2 E, 49.9 N
Nominal R_c (GV)	0.66–0.78	0.92–0.94	1.02–1.09
Measured R_c (GV)	0.54	0.68	0.79

TABLE 2

OBSERVED RATIO OF ALBEDO PROTONS TO DOWNWARD-MOVING PROTONS FOR DIFFERENT RIGIDITY BINS

R (GV)	Ratio
0.56–0.63	$(2.34 \pm 0.13)10^{-2}$
0.63–0.71	$(1.54 \pm 0.09)10^{-2}$
0.71–0.79	$(1.15 \pm 0.07)10^{-2}$
0.79–0.89	$(6.0 \pm 0.5)10^{-3}$
0.89–1.0	$(3.5 \pm 0.4)10^{-3}$

The overall efficiency was determined from the fraction of particles that passed the selection criteria. Using samples of $z = 1$ and $z = 2$ particles, the percentage that passed each chosen criterion is shown along with the estimated error in Table 3, where the overall efficiency is the product of the fractions that passed the consecutively (from the top) applied cuts. The difference between the two samples in passing the criterion A is due to more $z = 1$ background particles. The difference in the fraction that passed the χ^2 cut is probably due to δ-rays and Coulomb scattering. In the extreme, delta rays cause the sum of the two arrival times at each end of the delay line to be too low, resulting in an event which appears as a multitrack event. In the intermediate case, the sum of the two arrival times may not be bad enough for the event to be rejected, but it would be bad enough to cause a high χ^2 and to affect the measured position.

The proton and helium spectra are shown in Figures 9*a* and 9*b*, respectively, along with the *IMP 8* satellite data for a 48 hr period (1987 August 21–22) that overlapped the LEAP flight (Reames 1990), previous balloon data (discussed in § 3.4), and a family of curves representing calculated spectra for various levels of solar modulation (discussed in § 3.5). The *IMP 8* satellite has been measuring the elemental composition of solar energetic particles since 1973 (McGuire, von Rosenvinge, & McDonald 1986), and additional data for the period 1987 March 1–July 1, near the 1987 solar minimum, has been reported by McDonald et al. (1990). The LEAP differential spectra at the top of the atmosphere were obtained by using semiempirical total reaction cross sections (Garcia-Munoz et al. 1987) to correct the measured spectra for attenuation in the matter above the MWPCs. The results agree qualitatively with the previous high-energy balloon data, but there are greater differences among the experiments than the statistical errors would permit. Therefore, it is necessary to discuss some of the potential sources of systematic error.

The errors for the deconvolved spectra were estimated by the same method used by Webber et al. (1987), i.e., the sum of the statistical errors and the errors associated with the incremental change resulting from the deconvolution process:

$$\sigma_{\text{deconvolved}} = (N_{\text{obs}} + |N_{\text{deconvolved}} - N_{\text{obs}}|)^{1/2} .$$

The errors, which are energy dependent, are indicated by error bars in Figures 9*a* and 9*b* if they are larger than the symbols used. Most of the errors, however, are $\sim 1\%$, i.e., smaller than the size of the symbols. The overall flux uncertainty depends mainly on the uncertainty in the overall instrument efficiency given in Table 3, which is about 12% for both protons and helium. The uncertainty in the exposure factor was 2%–3%, so the overall flux uncertainty would be $\sim 15\%$, which agrees with estimates by Golden (1990) based on results from repeated flights of the balloon-borne spectrometer. This overall flux uncertainty may shift the spectra up or down by as much as 15%, but it would not affect the spectral shapes.

3.4. *Spectra at High Energies (above* 10 GV)

Numerous experiments have been performed in the past to study protons and helium. However, few direct measurements significantly greater than 10 GV have been made, and none has covered the LEAP energy range (0.5–100 GV) with a single instrument. The LEAP differential spectra above 10 GV follow rigidity power laws with spectral indices of 2.74 ± 0.02 for protons and 2.68 ± 0.03 for helium. The comparable measurements shown in Figure 9 are (1) Webber et al. (1987), who observed the spectral index of 2.70 ± 0.05 for both protons and helium with the same magnet spectrometer in 1976 and 1979—both of these earlier flights had lower statistics at higher geomagnetic cutoff and somewhat higher maximum detectable rigidity for the raw data (90 GV and 120 GV, respectively, for the 1976 and 1979 flights); (2) Ryan et al. (1972), who observed spectral indices of 2.75 ± 0.03 for 50–1000 GeV per nucleon protons and 2.77 ± 0.05 for 20–800 GeV per nucleon helium using an ionization calorimeter; and (3) Smith et al. (1973), who reported spectral indices of 2.63 ± 0.08 and 2.47 ± 0.03, respectively, for protons and helium in the range 8.3–100 GV using a superconducting magnet spectrometer. Not shown in Figure 9 are the data of Verma et al. (1972), who reported a spectral index of 2.8 ± 0.15 for 22–150 GV helium using a permanent magnet with an emulsion stack.

3.5. *Solar Modulation*

The spherically symmetric model described by Gleeson & Axford (1968) and Fisk, Forman, & Axford (1973) has been used to describe the solar modulation of cosmic rays in the heliosphere. In this standard model the cosmic rays propagating through the solar wind are subjected to the following transport processes: (1) diffusion through the turbulent magnetic

TABLE 3

PERCENTAGE OF PARTICLES PASSING THE VARIOUS SELECTION CRITERIA

Selection Criteria	Charge 1	Charge 2
A. Trajectory reconstructible	89.7% ± 1.1%	99.6% ± 0.3%
B. At least six good x-chambers	62.4 ± 2.9	59.8 ± 5.0
C. Pass TOF check	68.8 ± 7.8	70.5 ± 9.9
D. At least threee good y-chambers	97.1 ± 1.2	97.2 ± 0.6
E. Pass χ^2 (x) cut	91.8 ± 1.4	82.2 ± 3.0
F. Pass χ^2 (y) cut	97.2 ± 0.1	97.6 ± 0.2
Overall	33.4 ± 4.1	33.0 ± 3.9

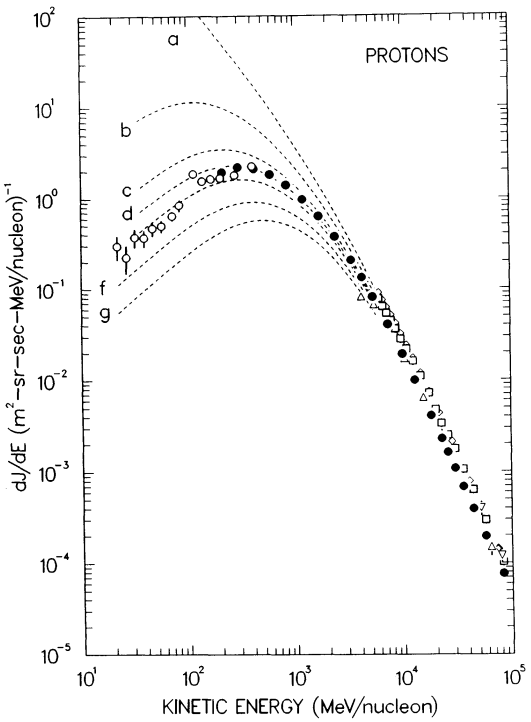

FIG. 9a

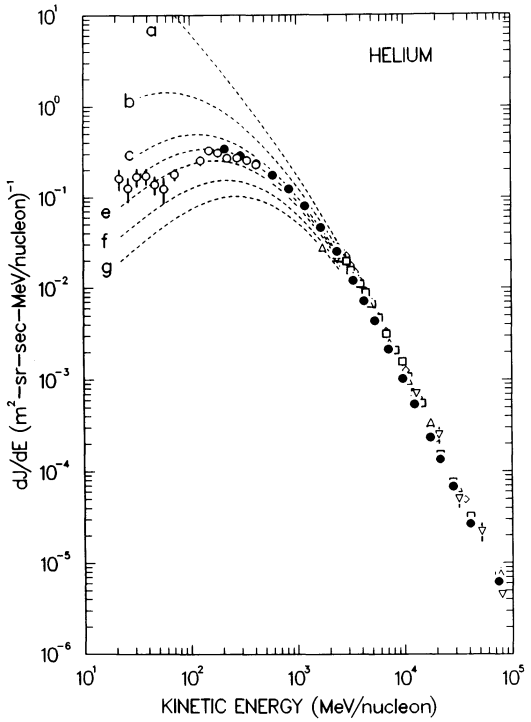

FIG. 9b

FIG. 9.—Differential energy spectra for cosmic-ray protons (*a*) and helium nuclei (*b*) measured in 1987 (*filled circles* for LEAP, *open circles* for *IMP 8*) along with the previous balloon measurements: *open diamonds* (1976 data), *open squares*, (1979 data), Webber et al. (1987); *inverted triangles*, Ryan et al. (1972); *upright triangles*, Smith et al. (1973). The dashed curves represent the local interstellar and modulated spectra with different amounts of modulation indicated by the modulation parameter ϕ: a, local interstellar spectra (no modulation); b, $\phi = 200$ MV; c, $\phi = 400$ MV; d, $\phi = 500$ MV; e, $\phi = 600$ MV; f, $\phi = 800$ MV; g, $\phi = 1000$ MV.

fields; (2) convection by the outward motion of the field embedded in the solar wind; and (3) adiabatic deceleration by the expansion of the fields as they propagate away from the Sun. With the solar modulation model thus specified, we have assumed that the local interstellar spectra of protons and helium at the heliospheric boundary are described by our high energy spectra, $\sim AR^{-2.74}$ and $\sim BR^{-2.68}$, respectively, and we have modulated those spectra to obtain the best fit to the 1987 LEAP measurements.

The normalization constants A and B were chosen to match the LEAP data near 100 GeV per nucleon, where the modulation effect is negligible. The diffusion coefficient was chosen to be $k = C_0 \beta R$, where C_0 can be adjusted to get the best agreement between the calculated and observed spectra. A heliospheric boundary distance $r_B = 50$ AU and a solar wind speed $v = 400$ km s^{-1} were assumed in the calculations.

Our numerical solutions to the steady state spherically symmetric Fokker-Planck equation (Fisk et al. 1973) at radius $r = 1$ AU, i.e., the modulated spectra, have been compared with the LEAP proton and helium measurements. The resulting sets of modulated spectra, representing various modulation parameters, are shown with the experimental data in Figures 9*a* and 9*b*. The coefficient $C_0 = 1.96 \times 10^{22}$ cm^2 s^{-1} GV^{-1} gives the best fit to the LEAP data. This corresponds to the solar modulation parameter $\phi \cong 500$ MV, where

$$\phi = \frac{1}{3} \int_{r_1}^{r_B} \frac{v}{k} \, dr \, .$$

Allowing for the 15% systematic uncertainty in the LEAP absolute fluxes, the modulation parameter was determined to be $\phi = 500 \pm 75$ MV. The low-energy *IMP 8* data apparently give better agreement with $\phi = 600$ MV. This small discrepancy may be attributed to the interstellar spectral form not following the rigidity power law precisely at low energies. No effort was made to fit the LEAP and *IMP 8* data at the same time. The energy loss due to solar modulation is $\Delta E = ze\phi$ for charge z particles. Taking different r_B or v did not change the result, i.e., $r_B v/C_0 =$ constant, which would be larger at times of higher solar activity, either from larger values of v/k or from increased distances, r_B, to the boundary.

The proton and helium spectra observed by LEAP soon after the 1987 March cosmic-ray intensity maximum near the solar minimum between the 21st and 22nd solar cycle (Shea & Smart 1990), and the *IMP 8* data (McDonald et al. 1990) for the period 1987 March 1–July 1 are compared with measurements from the 1977 and 1965 solar minima in Figures 10 and 11, which also show the 1969 solar maximum data for comparison. Figure 10*a* compares the LEAP proton data with the 1977 solar minimum measurements, while Figure 10*b* shows this comparison for the 1965 solar minimum. Likewise, Figure 11*a* compares the LEAP helium data with the 1977 solar minimum measurements, while Figure 11*b* shows the comparison for the 1965 solar minimum. The upper curves in Figures 10*a* and 11*a* represent modulation theory fits by Evenson et al. (1983) to the 1977 solar minimum measurements, while the upper curves in Figures 10*b* and 11*b* represents fits to the 1965 solar minimum measurements. The lower curves in the figures

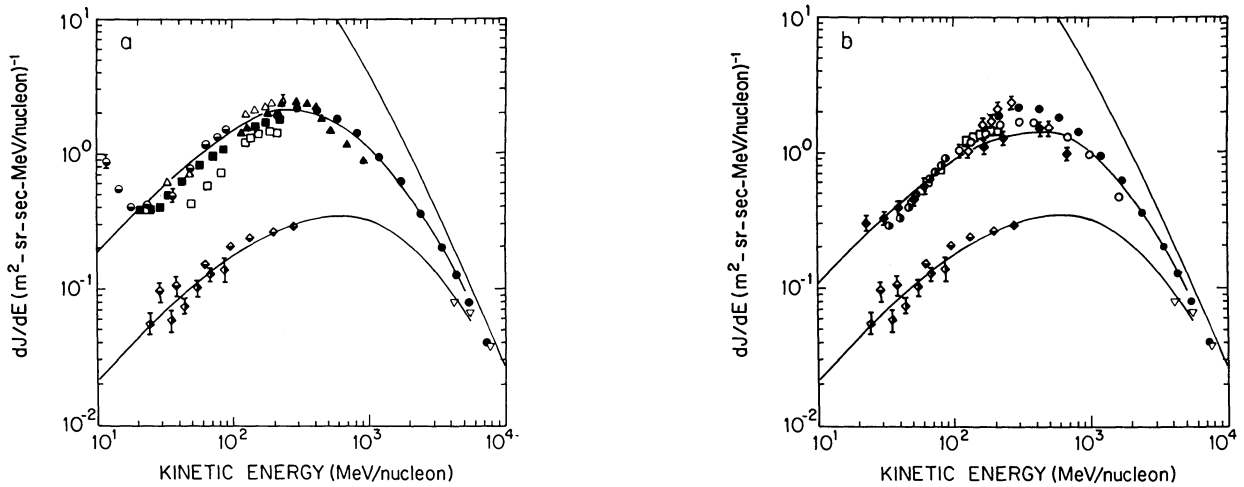

FIG. 10.—Comparison of the 1987 LEAP (*filled circles*) and *IMP 8* (*open squares*) proton spectra with measurements during the 1977 solar minimum (*a*) and 1965 solar minimum (*b*). For comparison, the 1969 solar maximum measurements are shown with the lower curves in both parts of the figure. The curves represent modulation theory fits by Evenson et al. (1983) to the 1977 (*a*) and 1965 (*b*) solar minimum measurements (*upper curves*) and the 1969 solar maximum measurements (*lower curves*). (*a*) Data for the 1977 solar minimum are *lower half-filled circles*, Evenson et al. (1983); *filled squares*, von Rosenvinge, McDonald, & Trainor (1979); *filled triangles*, Webber & Yushak (1979); *open triangles*, McDonald et al. (1979). Data for the 1969 solar maximum are *horizontally half-filled diamonds*, Garrard (1973); *vertically half-filled diamonds*, Hsieh, Mason, & Simpson (1971); *open inverted triangles*, Smith et al. (1973). (*b*) Data for the 1965 solar minimum are *open circles*, Ormes & Webber (1968); *open diamonds*, Rygg & Earl (1971); *filled diamonds*, Balasubrahmanyan et al. (1965); *vertically half-filled circles*, Fan, Gloeckler, & Simpson (1966). The 1969 data symbols are the same as in (*a*).

represent fits to the 1969 solar maximum measurements. The cosmic-ray fluxes were a bit higher in 1977 than during the previous 1965 solar minimum, whereas the absolute fluxes of protons and helium observed by LEAP in 1987 were approximately equal to the highest fluxes observed during 1977.

The solar modulation parameter ϕ for solar minimum has previously been estimated (Evenson et al. 1983) to be 300–600 MV by fitting the measured electron spectrum using the local interstellar electron spectrum deduced by Cummings, Stone, & Vogt (1973) from the Galactic nonthermal radio emission. It has also been estimated to be 450 $\pm$ 100 MV from the quartet of primary and secondary isotopes ^{1}H, ^{2}H, ^{3}He, and ^{4}He (Webber & Yushak 1983; Kroeger 1986). These estimates are in good agreement with our value of 500 MV. Therefore, as suggested by Webber (1987), rigidity power-law spectra appear to be reasonable forms for the proton and helium interstellar spectra above 200 MeV per nucleon.

3.6. *Proton-to-Helium Ratio*

Since higher energy cosmic rays escape more readily from the Galaxy, the spectral modification introduced by reacceleration would be energy-dependent. This effect should be especially noticeable for light elements, particularly protons and helium, whose interaction mean free paths are much longer than their escape mean free paths (Stephens & Golden 1989). The effects of reacceleration have been examined by comparing the LEAP observations with the expected p/He ratio calcu-

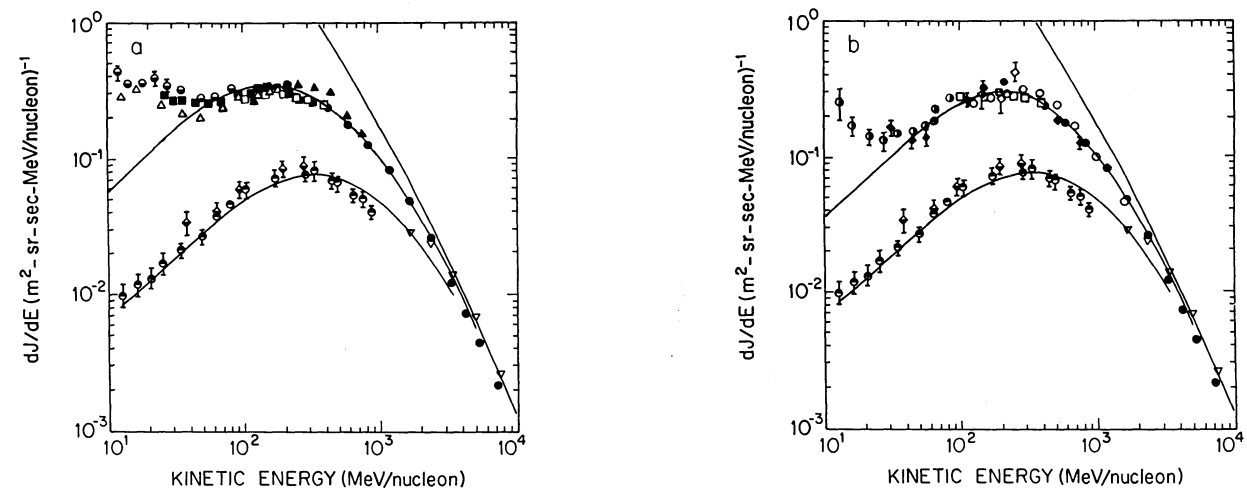

FIG. 11.—Comparison of the 1987 LEAP (*filled circles*) and *IMP 8* (*open squares*) helium spectra with measurements during the 1977 solar minimum (*a*) and 1965 solar minimum (*b*). For comparison, the 1969 solar maximum measurements are shown with the lower curves in both parts of the figure. The symbols and references to the data points and curves are the same as in Fig. 10, with one additional data point; *upper half-filled circles*, Mason (1972).

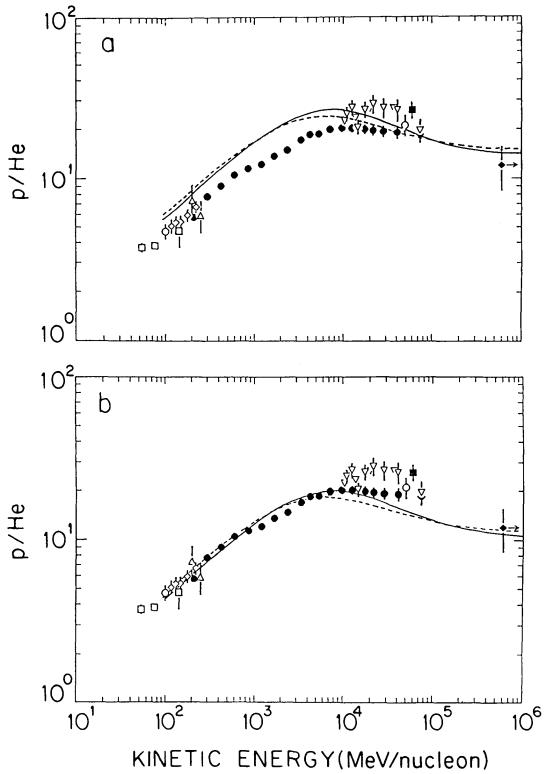

FIG. 12.—Proton-to-helium ratio as a function of energy. The experimental measurements are *filled circles*, this data from LEAP; *filled diamonds*, the JACEE data (Burnett et al. 1990) above 2 TeV per nucleon; *open circles*, Simpson (1983); *filled squares*, Ryan et al. (1972); *open diamonds*, Webber & Yushak (1983); *open squares*, *IMP 8* (Reames 1990); *open triangles*, Rygg & Earl (1971); *inverted open triangles*, Webber et al. (1987). The curves represent calculations of the *p*/He ratios near Earth with reacceleration (Stephens & Golden 1990): *solid lines*, rigidity spectra with rigidity dependent propagation; *dashed lines*, momentum spectra with momentum dependent propagation. The curves are normalized to the high-energy LEAP data in (*a*) and to the low-energy LEAP data in (*b*).

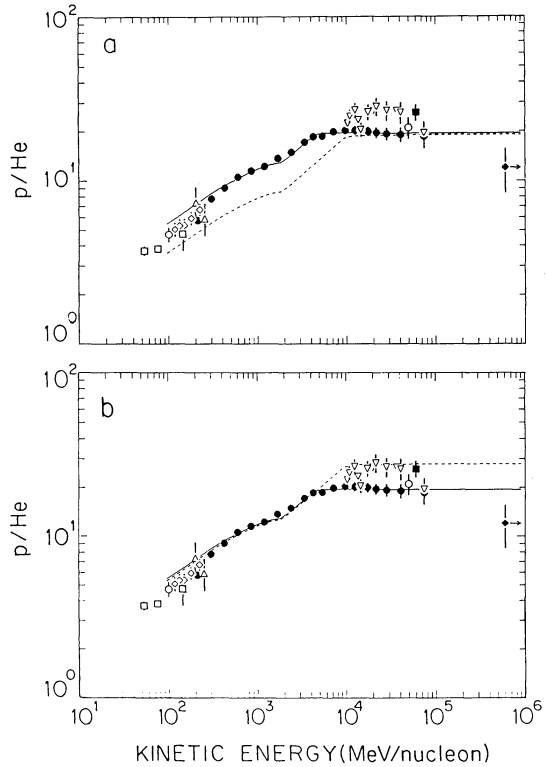

FIG. 13.—Proton-to-helium ratio as a function of energy. The symbols and references to the data points and curves are the same as in Fig. 12. The curves represent calculations of the *p*/He ratios near Earth without reacceleration. The curves in (*a*) are normalized to the high-energy LEAP data. The dashed curve in (*b*) is normalized to the low-energy LEAP data.

lated by Stephens & Golden (1990) based on the distributed reacceleration model of Wandel et al. (1987).

The *p*/He ratios from the LEAP experiment are shown in Figures 12 and 13, along with previous measurements of Webber et al. (1987), Ryan, Ormes, & Balasubrahmanyan (1972), Webber & Yushak (1983), Rygg & Earl (1971), Burnett et al. (1990), and the compiled data reported by Simpson (1983). In Figure 12, the experimental measurements are compared with the calculated sets of curves for the *p*/He ratios near Earth at solar minimum taking into account reacceleration. In order to facilitate the comparison, the calculated curves are normalized to the high-energy ($\sim$100 GeV per nucleon) LEAP data in Figure 12*a* and to the low-energy ($\sim$1 GeV per nucleon) LEAP data in Figure 12*b*. In both parts of Figure 12 the solid curves are based on rigidity-dependent propagation with power-law injection spectra in rigidity, while the dashed curves are for momentum-dependent propagation with power law spectra in momentum. Comparison of Figures 12*a* and 12*b* shows that when the curves are normalized to fit the high-energy data the calculated ratios are about 30% higher than the low-energy data, whereas when the curves are normalized to fit the low-energy data the calculated ratios are 20%–30% lower than the high-energy data. In the latter case, the discrepancy between the measurements and the calculation above a few GeV per nucleon becomes larger as the energy increases. However, an extrapolation of the curves to higher energies agrees with the Burnett et al. ratio 12 ± 3.6 above 2 TeV per nucleon.

Figure 13 compares the measurements with the calculated *p*/He ratios without reacceleration. The symbols and curves are the same as in Figure 12. Notice that the slope of the curves changes at two different energies which correspond to the same rigidity (5.5 GV) of proton and helium for the rigidity dependent propagation, and to the same momentum (11 GeV c^{-1}) of proton and helium for the momentum dependent propagation. When the curves are normalized to fit the high-energy data, as shown in Figure 13*a*, the calculated ratios corresponding to rigidity spectra with rigidity-dependent propagation (*solid curve*) agree well with the LEAP data. However, the dashed curve corresponding to momentum spectra with momentum-dependent propagation is about 35% lower than the measured ratios. When the curves are normalized to fit the low-energy data, as shown in Figure 13*b*, the solid curve again agrees well with the data while the dashed curve is about 40% higher than the high-energy LEAP data. Although the dashed curve agrees with some of the Webber et al. (1987) data points, its constant slope in the 4–11 GeV per nucleon interval does not agree with the measurements. It should be noted that the conclusion of Stephens & Golden (1990) that the propagation of cosmic rays is dependent on momentum was made on the basis of former measurements without the intermediate energy data provided by LEAP.

In summary, the comparisons in Figures 12 and 13 show that the data do not support reacceleration of the magnitude suggested for heavy nuclei by Wandel et al. (1987), but they do agree with the case of no reacceleration during propagation that is dependent on rigidity (Webber et al. 1987) and with an injection spectrum that is a power law in rigidity (Webber & Lesniak 1974).

4. SUMMARY AND CONCLUSIONS

The cosmic-ray proton and helium spectra have been measured in 1987 with a balloon-borne superconducting magnet spectrometer over a wide energy range with high statistics near the solar minimum between the 21st and 22nd solar cycle (Shea & Smart 1990). The effect of the changing geomagnetic cutoff was observed in the low-energy proton data throughout the flight, as the balloon's trajectory moved over the 0.66–1.10 GV range of nominal cutoff values calculated by Shea & Smart (1983). The measured cutoffs were consistently about 25% lower than the nominal cutoffs, but they generally agreed with earlier observations (Bingham et al. 1968).

The observed proton and helium absolute fluxes were approximately equal to the highest fluxes seen during the previous solar minimum in 1977. Above 10 GV the spectra can be represented by power laws in rigidity with spectral indices of 2.74 ± 0.02 for protons and 2.68 ± 0.03 for helium. Using these forms for the interstellar spectra, our measurements indicate that the modulation parameter was $\phi = 500 \pm 75$ MV during the 1987 solar minimum.

The observed p/He ratio does not support reacceleration of the magnitude suggested for heavy nuclei (Wandel et al. 1987). Moreover, our result agrees with the calculations of Stephens & Golden (1990) based on rigidity power-law injection spectra and rigidity-dependent propagation without reacceleration.

The authors owe special thanks to R. Golden for his contribution to this work and for his invaluable assistance in operating the Balloon Borne Magnet Facility. We thank the crew of the NASA National Scientific Balloon Facility for providing an excellent launch and recovery. We also thank J. Lloyd-Evans and A. Moats for their participation in the design, construction, and flight of the instrument, and J. Perko for providing the solar modulation code and useful discussions. Finally, we thank J. P. Wefel for his support and critical reading of the manuscript.

This work was supported by NASA under grants NAGW-1247 and NAGW-1027.

REFERENCES

Adams, J. 1972, Ph.D. thesis, Department of Physics, North Carolina State University
Balasubrahmanyan, V. K., Hagge, D. E., Ludwig, G. H., & McDonald, F. B. 1965, Proc. 9th Int. Cosmic Ray Conf. (London), 1, 427
Barkas, W. H., & Berger, M. J. 1964, Tables of Energy Losses and Ranges of Heavy Charged Particles (NASA SP-3013) (Washington, D.C.: NASA)
Bell, A. R. 1978a, MNRAS, 182, 147
———. 1978b, MNRAS, 182, 443
Bingham, R. G., Webber, W. R., Sawyer, D. M., & Ormes, J. F. 1968, Canadian J. Phys., 46, S1078
Blandford, R. D., & Ostriker, J. P. 1978, ApJ, 221, L29
———. 1980, ApJ, 237, 793
Burnett, T. H., et al. 1990, ApJ, 349, L25
Cowsik, R. 1980, ApJ, 241, 1195
Cummings, A. C., Stone, E. C., & Vogt, R. E. 1973, Proc. 13th Int. Cosmic Ray Conf. (Denver), 1, 335
Eichler, D. 1980, ApJ, 237, 809
Evenson, P., Garcia-Munoz, M., Meyer, P., Pyle, K. R., & Simpson, J. A. 1983, ApJ, 275, L15
Fan, C. Y., Gloeckler, G., & Simpson, J. A. 1966, Phys. Rev. Letters, 17, 329
Fisk, L. A., Forman, M. A., & Axford, W. I. 1973, J. Geophys. Res., 78, 995
Fransson, C., & Epstein, R. I. 1980, ApJ, 242, 411
Garcia-Munoz, M., Simpson, J. A., Guzik, T. G., Wefel, J. P., & Margolis, S. H. 1987, ApJS, 64, 269
Garrard, T. L. 1973, Ph.D. thesis, California Institute of Technology
Gleeson, L. J., & Axford, W. I. 1968, ApJ, 154, 1011
Golden, R. L. 1990, private communication
Golden, R. L., Badhwar, G. D., Lacy, J. L., & Zipse, J. E. 1978, Nucl. Instr. Meth., 148, 179
Golden, R. L., et al. 1973, Nucl. Instr. Meth., 113, 349
Golden, R. L., et al. 1990, Nucl. Instr. Meth., in press
Hsieh, K. C., Mason, G. M., & Simpson, J. A. 1971, ApJ, 166, 221
Ip, W. H., & Axford, W. I. 1985, A&A, 149, 7
Kota, J., & Owens, A. J. 1980, ApJ, 237, 814
Kroeger, R. 1986, ApJ, 303, 816
Mason, G. M. 1972, ApJ, 171, 139
McDonald, F. B. 1957, Phys. Rev., 107, 1386
McDonald, F. B., Lal, N., McGuire, R., & von Rosenvinge, T. 1990, Proc. 21st Int. Cosmic Ray Conf. (Adelaide), 6, 144
McDonald, F. B., Van Hollebeke, M. A. I., Trainor, J. H., & Lal, N. 1979, Proc. 16th Int. Cosmic Ray Conf. (Kyoto), 12, 330
McGuire, R. E., von Rosenvinge, T. T., & McDonald, F. B. 1986, ApJ, 301, 938
Moats, A. 1989, Ph.D. thesis, Department of Physics, University of Arizona
Ormes, J. F., & Webber, W. R. 1968, J. Geophys. Res., 73, 4231
Pennypacker, C. R., Smoot, G. F., Buffington, A., Muller, R. A., & Smith, L. H. 1973, J. Geophys. Res., 78, 1515
Reames, D. 1990, private communication
Ryan, M. J., Ormes, J. F., & Balasubrahmanyan, V. K. 1972, Phys. Rev. Letters, 28, 985
Rygg, T. A., & Earl, J. A. 1971, J. Geophys. Res., 76, 7445
Seo, E. S. 1991, Ph.D. thesis, Department of Physics and Astronomy, Louisiana State University
Shea, M. A., & Smart, D. F. 1983, Proc. 18th Int. Cosmic Ray Conf. (Bangalore), 3, 411
———. 1990, Proc. 21st Int. Cosmic Ray Conf. (Adelaide), 6, 13
Silberberg, R., Tsao, C. H., Letaw, J. R., & Shapiro, M. M. 1983, Phys. Rev. Letters, 51, 1217
Simpson, J. A. 1983, Ann. Rev. Nucl. Sci., 33, 323
Smart, D. F., Shea, M. A., & Gall, R. 1969, J. Geophys. Res., 74, 4731
Smith, L. H., Buffington, A., Smoot, G. F., Alvarez, L. W., & Wahlig, M. A. 1973, ApJ, 180, 987
Stephens, S. A., & Golden, R. L. 1989, Adv. Space Res., Vol. 9, No. 12, 93
———. 1990, Proc. 21st Int. Cosmic Ray Conf. (Adelaide), 3, 353
Stochaj, S. J. 1990, Ph.D. thesis, Department of Physics, University of Maryland
Streitmatter, R. E., et al. 1989, Adv. Space Res., Vol. 9, No. 12, 65
Streitmatter, R. E., et al. 1990, Proc. 21st Int. Cosmic Ray Conf. (Adelaide), 3, 277
Takasaki, F., Ogawa, K., & Tobimatsu, K. 1985, Nucl. Instr. Meth., 228, 369
Verma, R. P., Rengarajan, S. N., Tandon, S. N., Damle, S. V., & Yash Pal 1972, Nature, 240, 135
von Rosenvinge, T. T., McDonald, F. B., & Trainor, J. H. 1979, Proc. 16th Int. Cosmic Ray Conf. (Kyoto), 12, 170
Wandel, A., Eichler, D., Letaw, J. R., Silberberg, R., & Tsao, C. H. 1987, ApJ, 316, 676
Webber, W. R. 1987, A&A, 179, 277
Webber, W. R., Golden, R. L., & Stephens, S. A. 1987, Proc. 20th Int. Cosmic Ray Conf. (Moscow), 1, 325
Webber, W. R., & Lezniak, J. A. 1974, Ap&SS, 30, 361
Webber, W. R., & McDonald, F. B. 1964, J. Geophys. Res., 69, 3097
Webber, W. R., & Yushak, S. M. 1983, ApJ, 275, 391